Structure of rat BCKD kinase: Nucleotide-induced domain communication in a mitochondrial protein kinase

Mischa Machius*†, Jacinta L. Chuang*, R. Max Wynn‡, Diana R. Tomchick*, and David T. Chuang*†

Departments of *Biochemistry and ‡Internal Medicine, University of Texas Southwestern Medical Center, 5323 Harry Hines Boulevard, Dallas, TX 75390-9038

Edited by Susan S. Taylor, University of California at San Diego, La Jolla, CA, and approved August 3, 2001 (received for review May 3, 2001)

Mitochondrial protein kinases (mPKs) are molecular switches that down-regulate the oxidation of branched-chain α-ketoacids and pyruvate. Elevated levels of these metabolites are implicated in disease states such as insulin-resistant Type II diabetes, branched-chain ketoaciduria, and primary lactic acidosis. We report a three-dimensional structure of a member of the mPK family, rat branched-chain α-ketoacid dehydrogenase kinase (BCK). BCK features a characteristic nucleotide-binding domain and a four-helix bundle domain. These two domains are reminiscent of modules found in protein histidine kinases (PHKs), which are involved in two-component signal transduction systems. Unlike PHKs, BCK dimerizes through direct interaction of two opposing nucleotide-binding domains. Nucleotide binding to BCK is uniquely mediated by both potassium and magnesium. Binding of ATP induces disorder–order transitions in a loop region at the nucleotide-binding site. These structural changes lead to the formation of a quadruple aromatic stack in the interface between the nucleotide-binding domain and the four-helix bundle domain, where they induce a movement of the top portion of two helices. Phosphotransfer induces further ordering of the loop region, effectively trapping the reaction product ADP, which explains product inhibition in mPKs. The BCK structure is a prototype for all mPKs and will provide a framework for structure-assisted inhibitor design for this family of kinases.

The mammalian mitochondrial branched-chain α-ketoacid dehydrogenase (BCKD) complex catalyzes the oxidative decarboxylation of branched-chain α-ketoacids derived from leucine, isoleucine, and valine. This reaction is the rate-limiting step in the oxidative degradation of these branched-chain amino acids, leading to lipogenesis and energy production. A Mendelian-inherited metabolic block at this step results in the condition known as maple syrup urine disease or alternatively branched-chain ketoaciduria, which displays clinical phenotypes such as often-fatal ketoacidosis, neurological derangement, and mental retardation (1).

Similar to the related pyruvate dehydrogenase and α-ketoglutarate dehydrogenase complexes, the mammalian BCKD complex is organized about a cubic 24-mer core of dihydrolipoyl transacylase (E2), with multiple copies of heterotetrameric branched-chain α-ketoacid decarboxylase/dehydrogenase (E1), homodimeric dihydrolipoamide dehydrogenase (E3), BCKD kinase (BCK), and BCKD phosphatase attached through ionic interactions (2–6). The activity of the BCKD complex is regulated by a reversible phosphorylation/dephosphorylation cycle in response to dietary and hormonal stimuli (7). Phosphorylation of Ser-292 and Ser-302 in the α-subunit of E1 by BCK results in complete inactivation of E1 and, therefore, the BCKD complex (8).

BCK, together with pyruvate dehydrogenase kinases (PDKs), define a novel family of protein kinases, the mitochondrial protein kinases (mPKs) (9). PDK isoforms down-regulate the activity of the pyruvate dehydrogenase complex by phosphorylation of serine residues in its respective E1 component. The expression of the PDK4 isoform is elevated in patients with insulin-resistant type II diabetes, resulting in impaired glucose utilization (10). Although eukaryotic protein kinases usually exhibit homology to mammalian serine/threonine/tyrosine kinases, mPKs were shown to be distant relatives of protein histidine kinases (PHKs) (11–13). PHKs, along with their response regulator components, constitute the two-component signal transduction (TCST) systems (14–17). TCST systems represent the central signaling machinery in bacteria, and they also exist in some eukaryotes and Archeae (18). They respond to external stimuli, typically extracellular, resulting in autophosphorylation of the kinase component at an internal histidine (the H box). The high-energy phosphoryl group is then transferred to an aspartyl residue on a response regulator, which modifies cellular behavior by means of an effector domain. The structural hallmarks of PHKs are a characteristic kinase core composed of an ATP/ADP-binding domain, a phosphotransfer domain, and a dimerization domain (16). The dimerization domain is a helix–hairpin–helix motif that forms a four-helix bundle on dimerization. The H box is located either in the dimerization domain or in a separate four-helix bundle domain. A pronounced sequence similarity has given rise to the speculation that mPKs and PHKs share a common mechanism for phosphotransfer (19), yet all biochemical studies to date have failed to prove this hypothesis (20, 21), and the mechanism that is used by mPKs remains unclear.

Here we report the crystal structure determination of rat BCK in the presence and absence of nucleotides. The provided structural information explains the nucleotide-binding characteristics in mPKs and will serve as the basis for the rational design of inhibitors against the above-mentioned diseases.

Methods

Expression and Purification of BCK. Recombinant BCK was produced as described (20), except with a His_6-tag at the C terminus, and further purified by gel filtration chromatography using a Superdex S-200 column (Amersham Pharmacia) equilibrated in buffer A [50 mM Hepes (pH 7.5)/1 M NaCl/250 mM KCl/300 mM arginine/20 mM β-mercaptoethanol/1 mM benzamidine/2 mM $MgCl_2$/0.5 mM PMSF/10% (vol/vol) glycerol]. Purified BCK was concentrated to about 20 mg/ml and stored at −80°C.

Crystallization, Data Collection, Structure Determination, and Refinement. Crystals were grown at 20°C by means of the vapor diffusion method by mixing equal amounts of BCK {20 mg/ml

This paper was submitted directly (Track II) to the PNAS office.

Abbreviations: BCK, branched-chain α-ketoacid dehydrogenase kinase; E1, branched-chain α-ketoacid decarboxylase/dehydrogenase; E2, dihydrolipoyl transacylase; mPK, mitochondrial protein kinase; PDK, pyruvate dehydrogenase kinase; PHK, protein histidine kinase.

Data deposition: The atomic coordinates have been deposited in the Protein Data Bank, www.rcsb.org (PDB ID codes 1gjv, 1gkx, and 1gkz).

†To whom reprint requests should be addressed. E-mail: David.Chuang@UTSouthwestern.edu or Mischa.Machius@UTSouthwestern.edu.

The publication costs of this article were defrayed in part by page charge payment. This article must therefore be hereby marked "*advertisement*" in accordance with 18 U.S.C. §1734 solely to indicate this fact.

www.pnas.org/cgi/doi/10.1073/pnas.201220098

Table 1. Data collection, phasing, and refinement statistics

	Apo	ADP	ATPγS	SeMet		
Data collection						
Space group	$P4_22_12$, 1 molecule per asymmetric unit, ≈70% solvent content					
Unit cell, Å						
a = b	128.77	128.74	127.72	128.28	128.40	128.46
c	73.92	74.37	74.31	73.85	73.87	73.90
Energy, eV	Cu-K_α	12661.4	Cu-K_α	12659.7 (peak)	12658.7 (inflection)	12860.0 (remote)
Resolution, Å	35.5–2.98 (3.10–2.98)	40.8–2.29 (2.39–2.29)	37.0–2.70 (2.80–2.70)	40.6–2.70 (2.80–2.70)	45.3–2.70 (2.80–2.70)	45.4–2.90 (3.00–2.90)
Completeness	99.4 (94.5)	95.7 (85.3)	99.6 (96.8)	99.3 (100.0)	94.6 (96.9)	93.7 (95.9)
R_{merge}*, %	2.3 (78.5)	4.4 (60.6)	6.1 (58.2)	7.4 (66.9)	7.2 (77.1)	9.5 (70.8)
$I/\sigma(I)$	26.3 (2.4)	22.4 (1.7)	24.4 (2.0)	20.3 (2.4)	20.0 (1.9)	17.0 (2.2)
Multiplicity	8.2 (7.6)	4.5 (3.2)	4.6 (3.6)	5.5 (5.5)	5.8 (5.7)	5.9 (5.9)
Wilson B factor, Å^2	66.7	60.7	67.4	66.7	64.6	75.1
MAD phasing						
Anomalous scatterer				selenium (eight/nine possible)		
Resolution, Å				34.2–2.7		
Figure of merit				0.940 (after density modification)		
Refinement						
Resolution, Å	35.5–2.98	40.7–2.29	36.9–2.70			
No. of reflections R_{work}/R_{free}	11149/1542	29372/1427	15235/1430			
R_{work}/R_{free}, %	24.3/27.2	22.5/28.5	23.1/28.1			
Number of solvent molecules	13	105	31			
Average B factor, Å^2	59.4	62.4	53.1			
rmsd bond lengths, Å	0.010	0.012	0.011			
rmsd bond angles, °	1.50	1.70	1.67			

Data collection values are as defined in the program SCALEPACK (22). MAD phasing and model refinement values are as defined in the program CNS (23). rmsd, rms deviation.

*$R_{merge} = 100\,\Sigma_h\Sigma_i \mid I_{h,i} - \langle I_h \rangle \mid / \Sigma_h \Sigma_i I_{h,i}$, where the outer sum (h) is over the unique reflections and the inner sum (i) is over the set of independent observations of each unique reflection.

in buffer A, with or without Mg-ADP or Mg-adenosine 5′-[γ-thio]triphosphate (ATPγS)} and well solution [8% (wt/vol) PEG-6000/5% (vol/vol) ethylene glycol/1 M NaCl/20 mM β-mercaptoethanol]. Crystals were cryo-protected by step-wise transfer into 25 mM Hepes (pH 7.5)/125 mM KCl/150 mM arginine/1 mM $MgCl_2$/10 mM DTT/14% (wt/vol) PEG-6000/500 mM NaCl/2.5% (vol/vol) ethylene glycol/20% (vol/vol) glycerol. The seleno-methionine variant was produced in the *Escherichia coli* strain B834 (DE3) and crystallized in the same manner. Crystals were flash-cooled in liquid propane and kept at 100 K during data collection at beamlines 19ID and 19BM [Advanced Photon Source (APS), Argonne National Laboratory, Argonne, IL], for multiple anomalous dispersion (MAD) data and data from BCK/ADP co-crystals. Data from apo-BCK and BCK/ATPγS crystals were collected with a rotating anode (RU-300, Rigaku, Tokyo) and an R-AXIS-IV detector (Molecular Structure, The Woodlands, TX). Data were processed with the program HKL2000 (22). Structure solution was achieved by MAD phasing in CNS (23). After density modification (using CNS), models were constructed with the program O (24) and refined (using CNS). Nucleotides, a magnesium ion, and a potassium ion were added after the protein model was complete. Water molecules were added where stereochemically reasonable. Average individual B factors for all models are high (60–65 Å^2), but agree with the Wilson B factors for the individual data sets. The final models contain residues 38–379 with varying portions of two loops disordered to different degrees.

Potassium ions in ADP and ATPγS-bound BCK were identified based on their anomalous signal. Their presence was confirmed by replacing potassium with rubidium, which resulted in a strong peak at the position of the cation in an anomalous difference Fourier map. The surrounding ligand sphere exhibits characteristic metal-oxygen distances (2.8–3.1 Å; ref. 25). Refinement of the potassium ions resulted in B factors similar to those for the surrounding ligands. Data processing and refinement statistics are summarized in Table 1.

ATPase Activity Measurements. BCK fused to maltose-binding protein (21) was used for determining the ATPase activity of BCK in the absence and presence of cations as well as apo- and lipoylated E2 as described (26). The catalytic properties of MBP-BCK are unchanged compared with purified His_6-tagged BCK, but MBP-BCK exhibits higher solubility (20).

Results and Discussion

Overall Structure. Crystal structure determination of rat BCK in its apo-form, complexed with ADP and with ATPγS at resolutions of 2.98, 2.29, and 2.7 Å, respectively, reveals a homodimeric arrangement. The BCK monomer comprises two domains (Fig. 1). The first domain (referred to as the B domain, residues 1–186) primarily contains two parallel helix–hairpin–helix motifs that form a four-helix bundle (helices BH1, BH2, BH3, and BH4). The first helix in each motif is interrupted by a kink. The second domain (referred to as the K domain, residues 187–373) contains a five-stranded β-sheet (strands KB1, KB2, KB3, KB4, and KB5) opposed by a layer of three helices (KH1, KH2, and KH3) and harbors the nucleotide-binding site. A long loop (residues 303–339) that surrounds part of the nucleotide-binding site is disordered to varying degrees depending on bound nucleotide. The B and K domains are connected by a flexible linker (residues 182–194) that adopts different conformations in our BCK structures.

Structural Similarity to Protein Histidine Kinases and GHL ATPases. The two domains in BCK are also found in two-component signal transduction (TCST) systems (Fig. 2). The K domain is structurally similar to the nucleotide-binding domains of PHKs, as represented by crystal structures of CheA (27) and EnvZ (28). It is also found in the so-called GHL ATPases, represented by

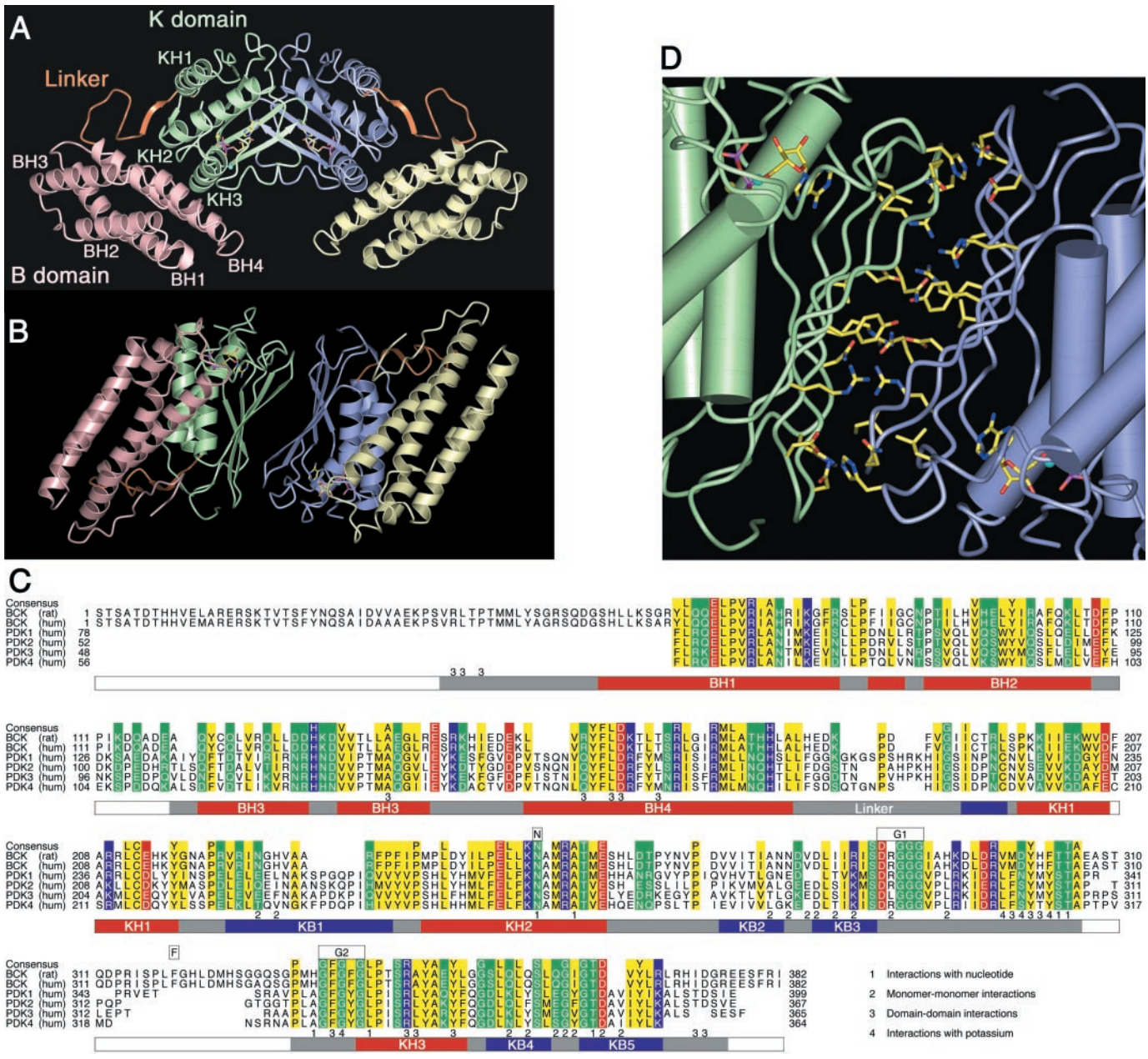

Fig. 1. The mammalian protein kinase BCK. (*A*) Overall view of the rat BCK dimer with the phosphotransfer reaction product ADP shown as ball-and-stick model. Strands in the K domain are not labeled. (*B*) Same as *A*, but rotated 90° around the horizontal line. All figures were made with BOBSCRIPT (46) and POVRAY (www.povray.org). (*C*) Sequence alignment of mitochondrial protein kinases. Similar residues are colored (yellow, hydrophobic; blue, basic; red, acidic; green, others). Residues observed in the rat BCK structure are depicted below the sequences (red, helices; blue, strands; gray, others); the conserved nucleotide-binding motifs are indicated above the consensus sequence. (*D*) Residues in the rat BCK dimer interface. Water molecules participate in dimer formation only at the periphery, but not in the core.

DNA gyrase B (GyrB; ref. 29), the chaperone Hsp90 (30), and the DNA mismatch repair ATPase MutL (31). A structure-based sequence alignment [performed in the program SWISSPDB-VIEWER (32)] between the K domains of BCK and the nucleotide-binding domains of the above listed proteins reveals 17% identity and 38% similarity for the 147 aligned residues for CheA, 13% identity and 28% similarity for the 127 aligned residues for EnvZ, 17% identity and 34% similarity for the 122 aligned residues for GyrB, 23% identity and 42% similarity for the 107 aligned residues for MutL, and 21% identity and 28% similarity for the 123 aligned residues for Hsp90. The B domain in BCK is structurally similar to four-helix bundle domains in TCST systems, as represented by CheA (33), ArcB (34), and Ypd1p (35). In PHKs, these domains either contain a conserved histidine that is used for phosphotransfer and/or they mediate dimerization. The function of this domain in mPKs is unclear. There is no detectable sequence similarity between BCK and PHKs in the B domain, whereas there is about 30% sequence identity and about 52% sequence similarity between BCK and PDKs. Because of the pronounced sequence similarity, the structure of BCK is expected to serve as a prototype for the mPK family (Fig. 1).

BCK Features an Intimate Domain Interface. The B and K domains within a BCK monomer interact with each other through two

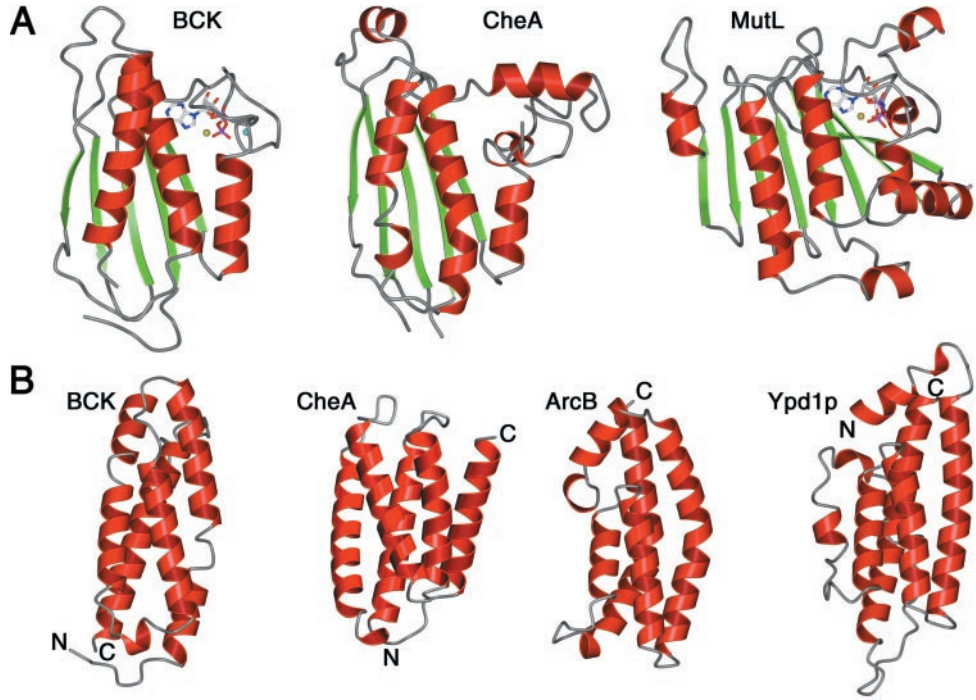

Fig. 2. Comparison of BCK with structurally related kinases and ATPases. (*A*) Nucleotide-binding domain. BCK with ADP, CheA ''empty'' (PDB ID code 1B3Q), and MutL with ADPNP (PDB ID code 1B63). (*B*) B domain. BCK, CheA-HPt (PDB ID code 1i5n), ArcB (PDB ID code 1A0B), and Ypd1p (PDB ID code 1C02).

interfaces (Fig. 3). The first interface is near the linker region and is formed by residues close to the N terminus (amino acids 39–42) and residues close to the C terminus (amino acids 373–374). A second, more intimate interface is located between helices BH4 and KH3 in close proximity to the nucleotide-binding pocket. It contains a hydrophobic cluster and aromatic stacking interactions (Ala-140, Leu-160, Tyr-301, His-302, and Phe-338), an ionic interaction between Arg-157 and Asp-300, and two polar interactions between the side chains of Asp-161 and Tyr-301 and between the carbonyl oxygen of Ala-140 and the side chain of His-302. The domain interface buries a total of about 2580 Å^2 of surface area.

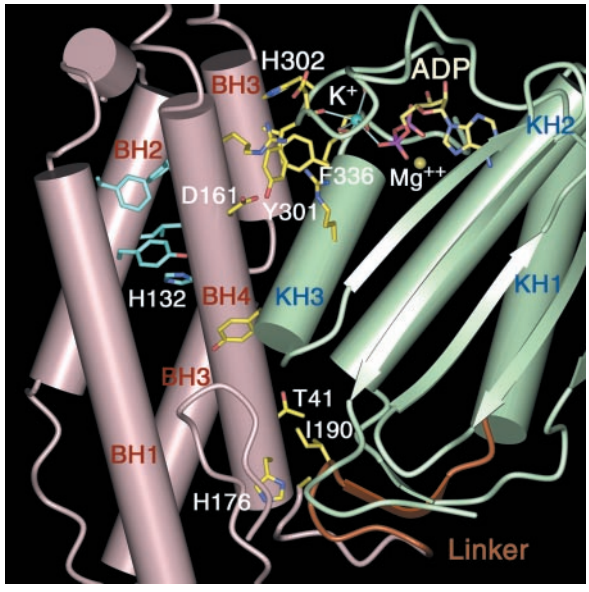

Fig. 3. Residues in the interface between domains B (pink) and K (green) in the ADP-bound state of the rat BCK monomer (carbon atoms in yellow) and in the hydrophobic core of the B domain (carbon atoms in cyan).

A Unique Mode of Dimerization. The BCK dimer in our crystal structure is formed by two crystallographically related molecules that interact through the concave surfaces of their K domains (Fig. 1). This mode of dimer formation is unprecedented for kinases that contain the histidine kinase-like ATP-binding domain. The dimer axis runs perpendicular to the helices and strands, and places the ATP-binding sites on opposite sides. The interface buries about 890 Å^2 of surface area per monomer and contains a number of hydrophobic and polar interactions, including ion pairs between Asp-278 and His-292 and between Arg-286 and Asp-365. BCK has a tendency to form tetramers in solution (21). A more detailed analysis using sedimentation equilibrium analytical ultracentrifugation showed that BCK exists in a dimer–tetramer equilibrium with a dissociation constant K_d = 1.5 μM (data not shown). Our crystal structure does not reveal the structural basis of BCK tetramerization, and its physiological significance remains unclear.

Nucleotide-Binding Pocket. The bound nucleotide forms contacts with conserved residues that belong to sequence motifs known as N, G1, F, and G2 boxes, originally identified in PHKs (Fig. 1; ref. 36). The phosphate groups protrude toward the solvent and are stabilized by the N-terminal portion of helix KH3 and the loop region that connects this helix with β-strand KB3. This loop region is analogous to the ''ATP lid'' of GyrB (29), MutL (37), and CheA (38). In BCK, it is largely disordered, even when nucleotide is bound, as in EnvZ (28), which supports the hypothesis that full ordering requires both nucleotide binding and specific protein–protein interactions (37–39). For BCK and PDKs, such interactions are probably provided by their respective E1 substrates and/or lipoyl-bearing domains of the E2 core (20, 21, 40).

Structural Basis for the Potassium Requirement of BCK. Binding of adenosine nucleotides in BCK is uniquely mediated by both

BIOCHEMISTRY

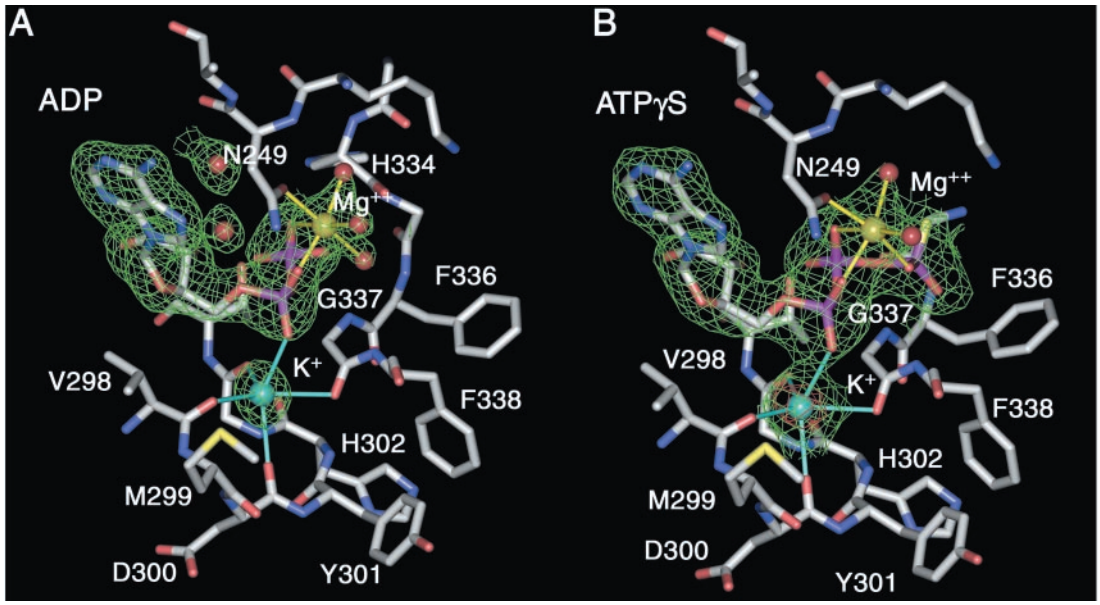

Fig. 4. Nucleotide-binding pocket of rat BCK with superimposed $2F_o - F_c$ simulated annealing omit electron density maps (green, contoured at 1.5 σ) calculated for potassium (cyan) and magnesium (yellow), as well as bound ADP (*A*) and ATPγS (*B*). An anomalous difference Fourier electron density map (red, contoured at 5 σ) is shown for the ATPγS-bound BCK structure. The side chain of Phe-303 has been removed for clarity.

magnesium and potassium (Fig. 4). The magnesium ion is bound to the conserved N249 (N box) and the phosphate moieties in the nucleotide. The potassium ion is liganded by the α-phosphate of the nucleotide and carbonyl oxygens of Val-298, Asp-300, Phe-303, and Gly-337. No electron density is observed in the potassium-binding site in apo-BCK, although potassium was present in the crystallization medium. The presence of potassium in the nucleotide-binding site explains the requirement of this metal for the kinase activity of BCK (41), as well as its ATPase activity (Table 2). Rubidium, but not sodium, can substitute for potassium. Residues Val-298 to Phe-303 belong to a loop whose main-chain conformation is virtually identical to a potassium-binding loop in a helix–hairpin–helix motif in human DNA polymerase β (42). It should be noted that potassium stimulates the autophosphorylation activity of CheA (43), but CheA does not contain the potassium-binding motif found in BCK, and the structural basis for this phenomenon is unclear. On the other hand, the potassium-binding motif found in BCK is present in MutL. It is therefore expected that potassium is involved in nucleotide binding in MutL, although this has not been reported.

Nucleotide-Induced Structural Changes in BCK. Nucleotide binding to the K domain of BCK induces structural changes that are transmitted via the B/K domain interface to the neighboring B domain (Fig. 5). In the apo-form, the region between Thr-304 and Phe-336 is disordered. Binding of ATPγS and potassium results in ordering of residues Thr-305–Ala-306 and Gly-335, adjacent to the potassium-binding site. This ordering leads to the formation of a quadruple aromatic stack between Tyr-301, His-302, Phe-336, and Phe-338. These residues alternate with potassium-binding residues, and their side chains are strategically placed in the interface between the B and K domains. On formation, the aromatic stack contacts the adjacent B domain,

Table 2. ATPase activity of BCK

Additions	ATPase activity*	
	k_{cat}, min^{-1}	%
None	0.1 ± 0.04	1
50 mM K^+	6.8 ± 1.5	100
50 mM Rb^+	5.0 ± 0.8	74
50 mM K^+ + apo-E2	7.2 ± 0.7	106
50 mM K^+ + lipoylated E2	15.6 ± 2.2	229

Results are averages of three determinations. The percent activities are expressed relative to BCK in the presence of potassium.
*ATPase activities were determined as described in *Methods*.

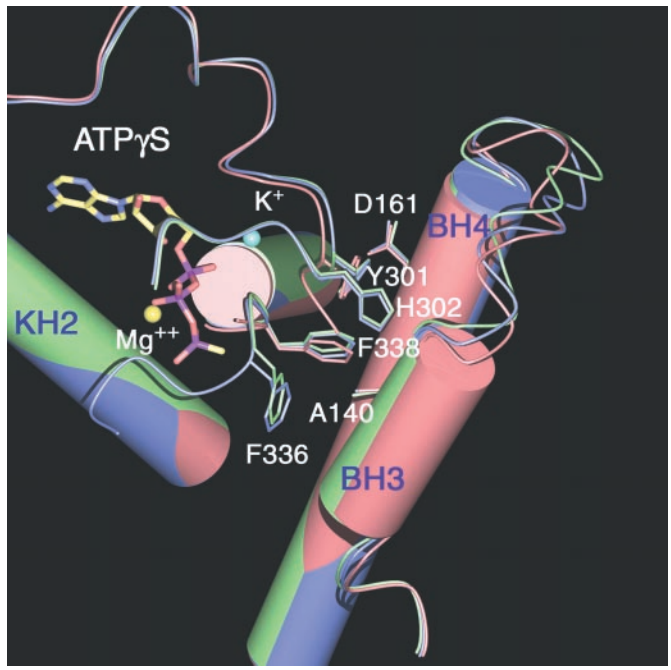

Fig. 5. Superposition of the apo-structure of rat BCK (red) with its ADP-bound (blue) and ATPγS-bound form (green). Nucleotide (ADP or ATPγS) binding orders H302 and F336 (electron density not visible in the apo-form) in the B/K domain interface to form a quadruple aromatic stack between Y301, H302, F336, and F338. Structural differences in the BH3 and BH4 helices between the apo and the nucleotide-bound states are depicted.

primarily through the Tyr-301/Asp-161 and His-302/Ala-140 interactions and causes a tilt in the top portion of the BH3/BH4 helix–hairpin–helix.

Structural Basis for Product Inhibition by ADP. The presence of the phosphotransfer reaction product ADP results in additional ordering of residues Pro-332–His-334 in the vicinity of the nucleotide-binding site (Fig. 5). The carbonyl oxygen of His-334 forms a hydrogen bond to the β-phosphate moiety, thereby effectively trapping the ADP (Fig. 4). This trapping mechanism explains the characteristic product inhibition observed in mPKs (44) and renders ADP analogs attractive as potential inhibitors for these enzymes. Atypical for protein kinases, BCK exhibits ATPase activity in the absence of its primary substrate E1. The product inhibition by ADP likely is a mechanism to prevent idle hydrolysis of ATP when no substrate is present. Reactivation of BCK requires the release of ADP, probably through specific removal of the loop region. The necessary interactions could be provided by the lipoyl-bearing domain of E2, which has been shown to stimulate the kinase activity of BCK (20, 21) as well as its ATPase activity (Table 2).

Domain Communication in BCK. The formation and stabilization of the domain interface on nucleotide binding effectively establishes a mechanism for communication between the B and K domains. This structural coupling explains the effects of certain site-specific mutations on enzyme activity. Replacing the central Tyr-301 by alanine in the domain interface leads to a 95% reduction in the catalytic activity of BCK (21). A similar effect was observed for the H121A mutation in *Arabidopsis thaliana* PDK (45). This conserved histidine (His-115 in human PDK1; His-132 in rat BCK) is located 25-Å distant from the ATP binding site and is buried in the predominantly hydrophobic core of the B domain (Fig. 3). Substitution by alanine creates a void that would be expected to destabilize the core, thereby affecting the structural integrity of this domain. Mutations that preserve the packing do not significantly lower the activity, as observed for the mutation H132N in BCK (R.M.W., unpublished data). Structural communication through the B/K domain interface explains the long-range effect of mutations in the core of the helical domain on the nucleotide-binding pocket, suggesting that proper interaction of the two domains is crucial for the integrity of the nucleotide-binding site. This aspect appears to be important for the function of mPKs, because the involved residues are well conserved.

We thank S. Hill for excellent technical assistance, and C. Brautigam, G. Rudenko, and E. Goldsmith for useful discussions. Use of the Argonne National Laboratory Structural Biology Center (SBC-CAT) beamlines at the Advanced Photon Source was supported by the U.S. Department of Energy, Office of Biological and Environmental Research, under Contract No. W-31-109-ENG-38. Support by the staff of the SBC-CAT is gratefully acknowledged. This work was supported by National Institutes of Health Grant DK-26758, Welch Foundation Grant I-1286, and American Heart Association Grant 95G-074R.

1. Chuang, D. T. & Shih, V. E. (2001) in *The Metabolic and Molecular Basis of Inherited Disease*, eds. Scriver, C. R., Beaudet, A. L., Sly, W. S. & Valle, D. (McGraw–Hill, New York), pp. 1971–2006.
2. Pettit, F. H., Yeaman, S. J. & Reed, L. J. (1978) *Proc. Natl. Acad. Sci. USA* **75,** 4881–4885.
3. Chuang, D. T., Hu, C. W., Ku, L. S., Markovitz, P. J. & Cox, R. P. (1985) *J. Biol. Chem.* **260,** 13779–13786.
4. Paxton, R. & Harris, R. A. (1982) *J. Biol. Chem.* **257,** 14433–14439.
5. Damuni, Z., Merryfield, M. L., Humphreys, J. S. & Reed, L. J. (1984) *Proc. Natl. Acad. Sci. USA* **81,** 4335–4338.
6. Reed, L. J., Damuni, Z. & Merryfield, M. L. (1985) *Curr. Top. Cell Regul.* **27,** 41–49.
7. Harris, R. A., Hawes, J. W., Popov, K. M., Zhao, Y., Shimomura, Y., Sato, J., Jaskiewicz, J. & Hurley, T. D. (1997) *Adv. Enzyme Regul.* **37,** 271–293.
8. Cook, K. G., Bradford, A. P., Yeaman, S. J., Aitken, A., Fearnley, I. M. & Walker, J. E. (1984) *Eur. J. Biochem.* **145,** 587–591.
9. Harris, R. A., Popov, K. M., Zhao, Y., Kedishvili, N. Y., Shimomura, Y. & Crabb, D. W. (1995) *Adv. Enzyme Regul.* **35,** 147–162.
10. Majer, M., Popov, K. M., Harris, R. A., Bogardus, C. & Prochazka, M. (1998) *Mol. Genet. Metab.* **65,** 181–186.
11. Popov, K. M., Hawes, J. W. & Harris, R. A. (1997) *Adv. Second Messenger Phosphoprotein Res.* **31,** 105–111.
12. Popov, K. M., Kedishvili, N. Y., Zhao, Y., Shimomura, Y., Crabb, D. W. & Harris, R. A. (1993) *J. Biol. Chem*. **268,** 26602–26606.
13. Koretke, K. K., Lupas, A. N., Warren, P. V., Rosenberg, M. & Brown, J. R. (2000) *Mol. Biol. Evol.* **17,** 1956–1970.
14. Stock, J. (1999) *Curr. Biol.* **9,** R364–R367.
15. Robinson, V. L., Buckler, D. R. & Stock, A. M. (2000) *Nat. Struct. Biol.* **7,** 626–633.
16. Stock, A. M., Robinson, V. L. & Goudreau, P. N. (2000) *Annu. Rev. Biochem.* **69,** 183–215.
17. Dutta, R., Qin, L. & Inouye, M. (1999) *Mol. Microbiol.* **34,** 633–640.
18. Plowman, G. D., Sudarsanam, S., Bingham, J., Whyte, D. & Hunter, T. (1999) *Proc. Natl. Acad. Sci. USA* **96,** 13603–13610.
19. Popov, K. M., Zhao, Y., Shimomura, Y., Kuntz, M. J. & Harris, R. A. (1992) *J. Biol. Chem.* **267,** 13127–13130.
20. Davie, J. R., Wynn, R. M., Meng, M., Huang, Y. S., Aalund, G., Chuang, D. T. & Lau, K. S. (1995) *J. Biol. Chem.* **270,** 19861–19867.
21. Wynn, R. M., Chuang, J. L., Cote, C. D. & Chuang, D. T. (2000) *J. Biol. Chem.* **275,** 30512–30519.
22. Otwinowski, Z. & Minor, W. (1997) *Methods Enzymol.* **276,** 307–326.
23. Brunger, A. T., Adams, P. D., Clore, G. M., DeLano, W. L., Gros, P., Grosse-Kunstleve, R. W., Jiang, J. S., Kuszewski, J., Nilges, M., Pannu, N. S., *et al*. (1998) *Acta Crystallogr. D* **54,** 905–21.
24. Jones, T. A., Zou, J. Y., Cowan, S. W. & Kjeldgaard, M. (1991) *Acta Crystallogr. A* **47,** 110–119.
25. Glusker, J. P. (1999) in *Protein: A Comprehensive Treatise*, ed. Allan, G. (JAI Press, Stamford, CT), Vol. 2, pp. 99–152.
26. Barylko, B., Binns, D. D. & Albanesi, J. P. (2001) *Methods Enzymol.* **329,** 486–496.
27. Bilwes, A. M., Alex, L. A., Crane, B. R. & Simon, M. I. (1999) *Cell* **96,** 131–141.
28. Tanaka, T., Saha, S. K., Tomomori, C., Ishima, R., Liu, D., Tong, K. I., Park, H., Dutta, R., Qin, L., Swindells, M. B., *et al.* (1998) *Nature (London)* **396,** 88–92.
29. Wigley, D. B., Davies, G. J., Dodson, E. J., Maxwell, A. & Dodson, G. (1991) *Nature (London)* **351,** 624–629.
30. Stebbins, C. E., Russo, A. A., Schneider, C., Rosen, N., Hartl, F. U. & Pavletich, N. P. (1997) *Cell* **89,** 239–250.
31. Ban, C. & Yang, W. (1998) *Cell* **95,** 541–552.
32. Guex, N. & Peitsch, M. C. (1997) *Electrophoresis* **18,** 2714–2723.
33. Mourey, L., Da Re, S., Pedelacq, J.-D., Tolstykh, T., Faurie, C., Guillet, V., Stock, J. & Samama, J.-P. (2001) *J. Biol. Chem.* **276,** 31074–31082.
34. Ikegami, T., Okada, T., Ohki, I., Hirayama, J., Mizuno, T. & Shirakawa, M. (2001) *Biochemistry* **40,** 375–386.
35. Xu, Q. & West, A. H. (1999) *J. Mol. Biol.* **292,** 1039–1050.
36. Alex, L. A. & Simon, M. I. (1994) *Trends Genet*. **10,** 133–138.
37. Ban, C., Junop, M. & Yang, W. (1999) *Cell* **97,** 85–97.
38. Bilwes, A. M., Quezada, C. M., Croal, L. R., Crane, B. R. & Simon, M. I. (2001) *Nat. Struct. Biol.* **8,** 353–360.
39. Brino, L., Urzhumtsev, A., Mousli, M., Bronner, C., Mitschler, A., Oudet, P. & Moras, D. (2000) *J. Biol. Chem.* **275,** 9468–9475.
40. Ono, K., Radke, G. A., Roche, T. E. & Rahmatullah, M. (1993) *J. Biol. Chem.* **268,** 26135–26143.
41. Shimomura, Y., Kuntz, M. J., Suzuki, M., Ozawa, T. & Harris, R. A. (1988) *Arch. Biochem. Biophys.* **266,** 210–218.
42. Pelletier, H. & Sawaya, M. R. (1996) *Biochemistry* **35,** 12778–12787.
43. Hess, J. F., Oosawa, K., Kaplan, N. & Simon, M. I. (1988) *Cell* **53,** 79–87.
44. Roche, T. E. & Reed, L. J. (1974) *Biochem. Biophys. Res. Commun.* **59,** 1341–1348.
45. Thelen, J. J., Miernyk, J. A. & Randall, D. D. (2000) *Biochem. J.* **349,** 195–201.
46. Esnouf, R. M. (1999) *Acta Crystallogr. D* **55,** 938–940.